Eur Biophys J (2004) 33: 29–37
DOI 10.1007/s00249-003-0339-2

ARTICLE

Jung-Chi Liao · Sean Sun · David Chandler
George Oster

The conformational states of Mg·ATP in water

Received: 21 March 2003 / Revised: 4 June 2003 / Accepted: 6 June 2003 / Published online: 7 August 2003

Abstract The conformational equilibria of Mg·ATP in solution is studied using molecular dynamics (MD) augmented with umbrella sampling methods. Free energy comparisons show that the Mg^{2+} ion is equally likely to coordinate the oxygens of the two end phosphates, or of all three phosphates. The MD trajectories reveal two major degrees of freedom of the Mg·ATP molecule in solution, and we compute the free energy as a function of these variables, and determine its elastic properties. Comparing the free energy function with several crystallographic structures of ATP analogs, we find that the crystal structures correspond to states where ATP would be elastically strained. The average water density around Mg·ATP is investigated to show the average number of hydrogen bonds and the hydrophobicity.

Introduction

Adenosine triphosphate (ATP) is a universal fuel for living systems. Protein motors such as myosin, kinesin, ATP synthase, and various AAA proteins (ATPases Associated with various cellular Activities), use ATP as the energy source to power their conformational changes. Understanding the transduction process between chemical energy and mechanical work is crucial to understanding the mechanisms of all these biological processes. The path to this understanding would be aided by a more complete description of the properties of Mg·ATP in solution, for this is the form that is captured by the catalytic sites of ATPases.

J.-C. Liao · S. Sun · G. Oster (✉)
Departments of Molecular and Cellular Biology and ESPM,
University of California, 201 Wellman Hall,
Berkeley, CA 94720-3112, USA
E-mail: goster@nature.berkeley.edu

D. Chandler
Department of Chemistry,
University of California,
Berkeley, CA 94720-3112, USA

The docking of ATP into the catalytic site is necessarily accompanied by dehydration of the nucleotide and the catalytic site, for water molecules must be released into solution from each putative hydrogen bonding site before the enzyme–ligand bond can form. Thus, understanding the process of ATP binding must rely on quantitative estimates of ATP interaction energies with water and the enzyme amino-acid residues. To understand the initial binding step, a realistic description of the ATP molecule in its various conformations is necessary. This paper reports on such a description obtained through molecular dynamics (MD) simulation augmented with the umbrella sampling method. The conformations considered are those for ATP solvated in water. The predominant protonated structure of ATP at pH = 7 is used (the chemical structure is shown in Fig. 5 of Appendix A). Two parameters sets, CHARMM parameter set (Pavelites et al. 1997) (MacKerell et al. 1998) and Minehardt parameter set (Minehardt et al. 2002), were used in the simulation. The details of the simulation are available in Appendix B.

Coordination of the Mg^{2+} ion

Experiments using ^{31}P NMR, chemical shifts, and coupling constants from various sources have sought to determine how Mg^{2+} coordinates with ATP in solution, but the results have been equivocal. Some experiments suggest that Mg^{2+} coordinates one oxygen atom from each of the three phosphates, although somewhat weakly for the α-phosphate (Kuntz et al. 1973; Mildvan 1987). Other experiments suggest that Mg^{2+} coordinates one oxygen atom from the γ-phosphate and one oxygen atom from the β-phosphate (Cohn et al. 1962).

In our simulations, a threshold length of 2.2 Å is used to determine which oxygen atoms are coordinated to the Mg^{2+} atom. Interestingly, the coordination depends on the initial conditions of the molecule. That is, simulations starting from the two coordination state (Mg^{2+} coordinating β- and γ-phosphates) persist for

more than 1 ns; starting from the three coordination state (Mg^{2+} coordinating α-, β- and γ-phosphates), the coordination remains in this three coordination state for more than 1 ns. Therefore, there is a high barrier between these two states so that they do not easily switch. For all the coordinated oxygen atoms of ATP in the simulations, the sampling distributions all peak at 1.8–1.85 Å from the center of the Mg^{2+} atom, with standard deviation less than 0.055 Å. All other uncoordinated atoms are 3 Å away from the center of the Mg^{2+} atom. These distributions validate the coordination threshold of 2.2 Å we used.

In order to understand the preference of these two states, we carried out an umbrella sampling study to connect these two coordination states (Chandler 1987; Frenkel et al. 2002). Because the only configurational difference between these two states is the Mg^{2+} coordination to one oxygen atom of the α-phosphate, we used the distance between this oxygen atom and Mg^{2+} as the order parameter, and constrained other oxygen atoms so that no extra oxygen atoms could be coordinated in each umbrella sampling window. By connecting the free energy in different windows, we can plot the free energy curve between these two states as shown in Fig. 1. A barrier of $\approx 18\ k_BT$ separates these two states. However, the order parameter we chose may not reflect the real transition path between these two coordination states. Thus the energy barrier along the real transition path might be lower than the one we obtained. Nevertheless, the barrier must be significant in order for the states to be stable over the simulation times. The free energy difference between the two states is only of the order of $1\ k_BT$. The curve shown in the figure was obtained using the CHARMM parameter set, but the curve obtained from the Minehardt parameter set is practically the same. These simulations suggest that Mg^{2+} is equally likely to coordinate β-, γ-phosphates or α-, β-, γ-phosphates. This may explain why there is still controversy in the experimental results. In the following simulation results for Mg·ATP, only the state where Mg^{2+} coordinates to β-, γ-phosphates was explored. The coordination for Mg·ADP has also been investigated and is discussed in Appendix C.

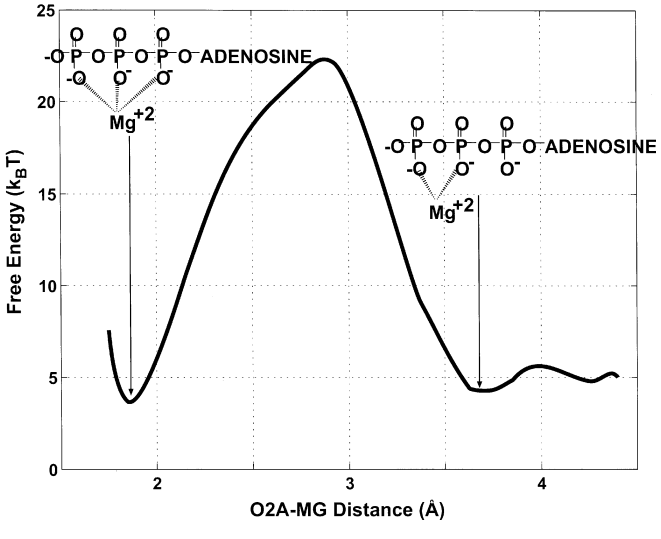

Fig. 1 The free energy between the state where Mg^{2+} coordinates α-, β-, γ-phosphates and the state where Mg^{2+} coordinates β-, γ-phosphates. The results were obtained by umbrella sampling using CHARMM parameters

The conformational equilibria of Mg·ATP in solution

A body-fixed coordinate system is placed on the adenine ring, which does not experience significant distortions in the simulation. Several dihedral angles are involved in the motion of the molecule. In terms of largest conformational changes of the molecule, the detailed changes in these dihedral angles all result in the deformations of the terminal atoms. The trajectory points of the γ-phosphorus relative to the reference frame form a "bowl" shape (see Appendix D), suggesting that the motion can be described by a simple spherical coordinate system. Using the least squares method we located a spherical coordinate center for this "bowl" of points. This spherical center is statistically the center of motion of the γ-phosphorus and it reflects the collective effect of all the intervening dihedral angles. The bowl is "thin" since the trajectory points measured from this center are roughly the same, with mean radius $\langle r \rangle = 8.92$ Å and standard deviation of the radius of 0.45 Å. Because variations in radius, r, are small, we use the circumferential angle, θ, and the azimuthal angle, Φ, as the primary conformational coordinates. This spherical coordinate system is shown in Fig. 2.

The free energy function

Based on statistics collected with umbrella sampling, the free energy function in the θ–Φ coordinates can be estimated by the histogram method (Frenkel et al. 2002). For comparison, the free energy surfaces for Mg·ATP and Mg-ADP using straightforward MD simulations are given in Appendix E. Binning the variables θ and Φ gives the distribution $p(\theta, \Phi)$, from which the free energy function is constructed, $F(\theta, \Phi) = -k_BT \ln p(\theta, \Phi)$. By subtracting the imposed potential energy from each sampling window, we connect each individual free energy surface together to obtain the global free energy surface (Ferrenberg et al. 1989). The free energy contour projected onto the (θ, Φ) base plane for Mg·ATP in solution using CHARMM parameters is shown in Fig. 3A. The low free energy region (i.e., the region of the preferred configurations of Mg·ATP in solution) is between $\theta \approx 30°$ to 40°, and $\Phi \approx -15°$ to $+15°$. Accumulated averages were carried out to demonstrate the approach to an equilibrated average, and the error in the free energy is of order $0.2\ k_BT$ or smaller.

Figure 3A also shows the locations of the γ-phosphorus of several ATP-analog molecules in different

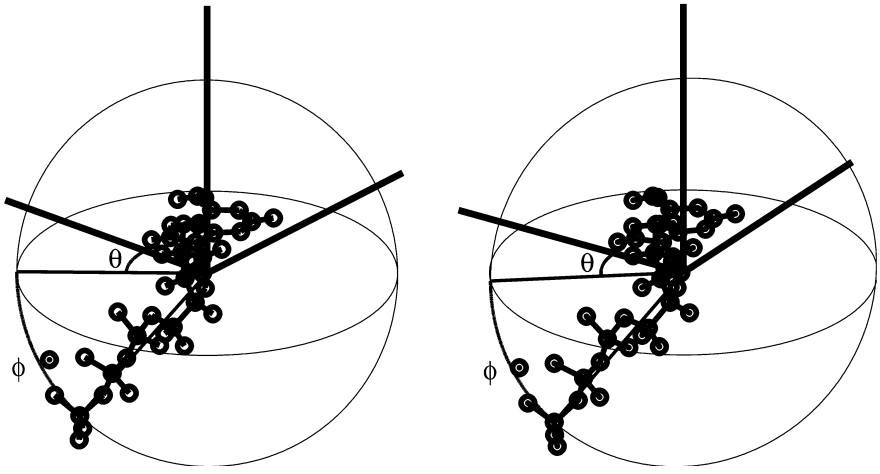

Fig. 2 Stereo view of location of the γ-phosphorus in the θ–Φ coordination. θ is the circumferential angle in the original x–y plane and Φ is the azimuthal angle. The center of the spherical coordinate is defined by least squares from the distance of sampling points

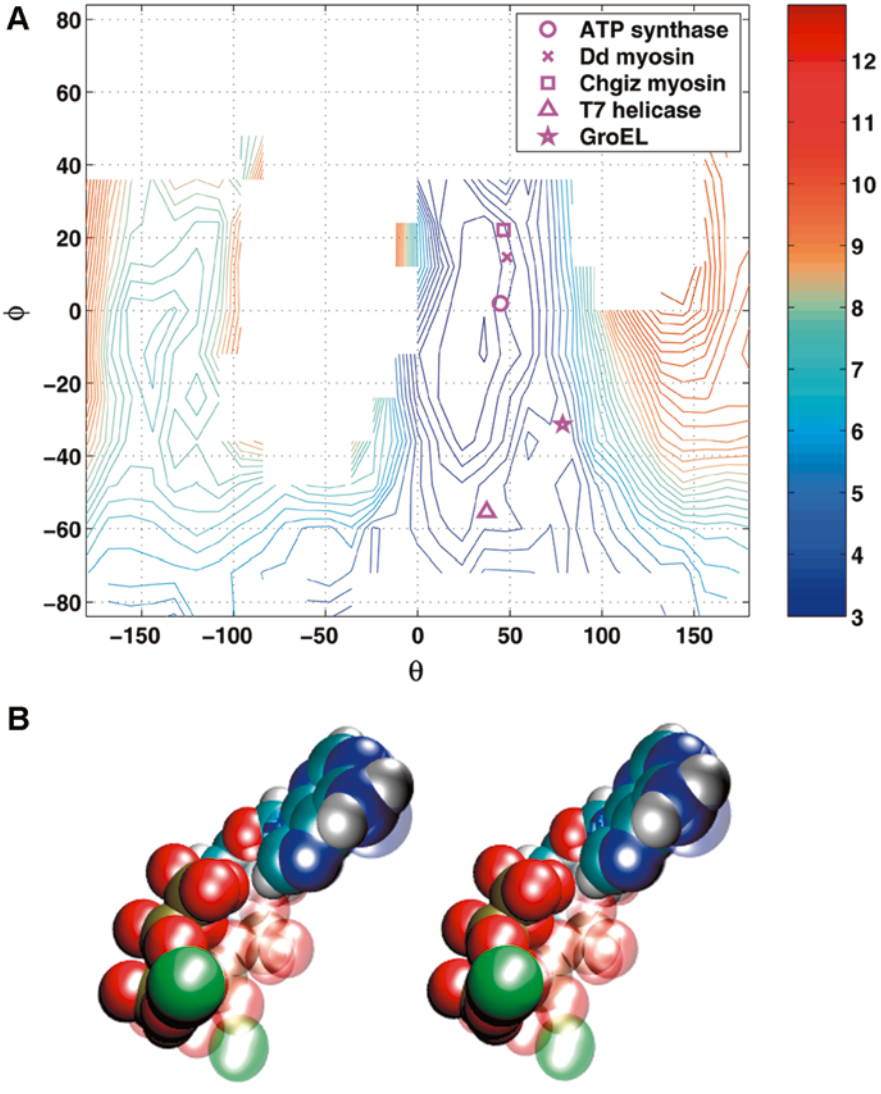

Fig. 3 **A** The free energy contour map of Mg·ATP in water mapped to the θ–Φ plane with locations of the ATP-analog crystal structures marked. The map was obtained by umbrella sampling using CHARMM parameters. The marked crystal structures are from the PDB coordinates 1BMF (ATP synthase), 1MMD (Dictyostelium Discoideum myosin), 1BR4 (chicken myosin), 1E0J (T7 gp4 helicase), and 1DER (GroEL). **B** Stereo view of Mg·ATP for the configuration close to the minimum free energy ($\theta = 35.6°$, $\Phi = -10.2°$) and the Mg·ANP of the ATP synthase crystal structure. The minimum energy configuration is shown opaque and the crystal structure is shown transparent. The coordination is defined as in Fig. 2, so that the adenine rings overlap each other. The triphosphate angles θ and Φ are shifted, indicating the strained configuration in the crystal structure

crystal structures. The ATP-analog molecules in proteins are all located in the energy well around $\theta \approx 35°$, but none are at the point we have estimated as the minimum free energy of ATP in solution. This suggests that, in the crystal, these ATP-analogs either reside in strained states, or their minimum energy configurations are

different than ATP because of their different structures. The figure shows the ATP molecules in ATP synthase and two kinds of myosins are in the states close to each other, while in T7 helicase and GroEL chaperonin they are in other distinct states. Figure 3B shows a stereo view of Mg·ATP for the configuration close to the minimum free energy ($\theta = 35.6°$, $\Phi = -10.2°$) and Mg-ANP of the ATP synthase crystal structure. The minimum energy configuration is shown opaque and the crystal structure is shown transparent. The configuration of Mg-ANP of ATP synthase is used because it is the one closest to the global minimum free energy. By the coordination described above, the adenine rings overlap each other. The triphosphate angles θ and Φ are shifted, indicating the strained configuration in the crystal structure. Thus the ATP analogs appear to possess different configurations in different protein catalytic sites, and therefore are in different strained states. However, according to the force field parameterization we have employed, the free energies of the strained states range only between 1 to 3 k_BT above the minimum. Thus bond strains may not play a major role in achieving the transition state leading to hydrolysis.

The elastic properties of Mg·ATP

Our studies suggest that, in different crystal structures, the enzyme-bound nucleotides are mostly in strained states. Thus the elastic properties of the nucleotide may play a role in coordinating adjacent atoms and motifs in the catalytic site. The free energy surface obtained above represents the flexibility of the molecule in solution. In particular, the ATP molecule behaves as an anisotropic mechanical beam bending in three-dimensional space, whose elastic properties vary in different directions. Around the minimum free energy in Fig. 3, we obtain that the effective elastic constant in the Φ direction (keeping θ constant) is about 25 pN nm^{-1}. Similarly, we fit a parabolic curve to estimate the effective elastic constant k_θ in the θ direction as 35 pN nm^{-1} (see Appendix F). The elastic properties considered here are those in the basin around the free energy minima, where most of the observed crystal structures are around.

We have shown that nucleotide analogs in various crystal structures are mostly in a strained state. The resulting strain, as shown in Fig. 3, is the accumulated effects of all the surrounding hydrogen bonding and other electrostatic forces. An elastic energy study of F_1-ATP synthase has shown that the formation of hydrogen bonds between the ATP molecule and the residues in the catalytic site distort the β-sheet that adjoins the catalytic site, leading to elastic energy storage in the β-sheet adjacent to the binding site (Sun et al. 2002). The elastic constants in the hinge-bending model of the β-subunit are 4–10 pN nm^{-1} (Wang et al. 1998). Compared to the elastic properties we obtained, the β-sheet is more flexible than the Mg·ATP molecule. The induced fit driven by the hydrogen bonding forces between the Mg·ATP molecule and the corresponding residues in the catalytic site deform the protein itself more than the ATP molecule. Thus the energy of hydrogen bond formation is transferred more to the protein than to the ATP molecule. The local strains in the catalytic site propagate globally to the β-sheet and other subunits so that the change in the strain field around the catalytic site when Mg·ATP binds to the enzyme provides additional insight into the protein motions during the catalytic cycle.

The average water density around Mg·ATP

The distribution functions shown in Fig. 4 give the average water densities at various locations around Mg·ATP as predicted from the Minehardt parameter set. Simulations with CHARMM parameters give similar results. The horizontal axis is the distance from the indicated atoms of the Mg·ATP molecule to oxygen atoms of water molecules. The atoms in the figure are selected because they represent different patterns of distribution functions. All atom numbers shown in the figure follow the numbering in CHARMM and are illustrated in Appendix A. The average water density was estimated from the number of water molecules per unit volume within a certain distance interval, averaged over a 2-ns trajectory. To facilitate reading the figure the density of each atom is shifted by 1 on the y-axis.

Most of the distribution functions shown in this figure have water density peaks ranging from 1.8 to 3.1 Å. These peaks correspond to the first layer water shell forming hydrogen bonds with the Mg·ATP

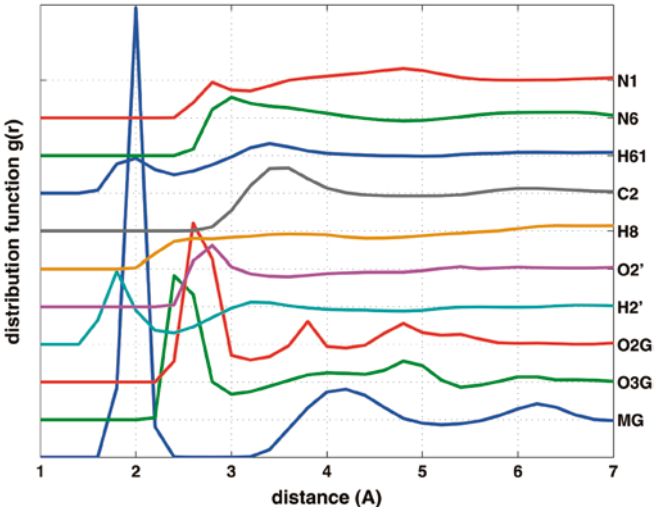

Fig. 4 The water density around selected atoms of Mg·ATP. The x-axis is the radial distance from the atom (with the atom name shown on the right). The distribution functions are estimated from the number of water molecules within a certain distance interval. For visulalization, the density of each atom is shifted by 1 on the y-axis. The data is obtained from averaging over 2-ns simulation runs

molecule. In the adenine ring, all the nitrogen atoms, N1, N3, N6 (the bound H61 and H62), and N7 are the potential hydrogen bonding sites. In double strand DNA, adenine forms two hydrogen bonds at the sites of N1 and one of the hydrogen atoms from N6 (H61 or H62) with the corresponding thymine. As shown in Fig. 4, the distribution function of atom N1 has a small peak around 2.8 Å, the average distance of an O–H··N hydrogen bond. The reason this peak is relatively small may be the small area accessible to solvent and the blocking of nearby water structure. For atom H61, a peak around 2 Å is observed. This is the N–H··O hydrogen bond including atom N6, and the distribution function of atom N6 shows a peak around 3 Å. The distribution functions of N3 and N7 are similar to that of N1, with higher peaks at 2.8 Å. For atom C2, a peak is shown at 3.5 Å. This distance corresponds to the van der Waals contact radii. The distribution function of H8 shows no peak at all, indicating that there is no coordinated water around this atom. Without a clear first shell of water molecules within 3.1 Å, the threshold of hydrogen bonds, C2 and H8 demonstrate the hydrophobic effect. In the ATP molecule, including adenine and ribose, distribution functions of all carbon atoms and hydrogen atoms bound to these carbon atoms show hydrophobic characteristics similar to those shown for C2 and H8. In the ribose ring, two hydroxyl groups and the oxygen atoms O4' are potential hydrogen bonding sites. Distribution functions of O2' and H2' are shown in Fig. 4. They are analogous to those of N6 and H61 shown above, with the peak for atom O2' at 2.8 Å, close to the average O–H··O hydrogen bond length of 2.7 Å.

The distribution functions of atoms in the triphosphate all show high peaks below 3 Å. As examples, we illustrate those for atoms O2G and O3G in Fig. 4, both from the γ-phosphate. The high peaks represent more than one water molecule coordinated in the first shell by the oxygen atoms of the triphosphate; possibly the coordinated water molecules are concentrated in a narrow range of distances. Comparing the distribution functions of O2G and O3G, the first shell peaks are at different places. In the simulation, O2G is one of the oxygen atoms coordinated by Mg^{2+}. Thus, the hydrogen bonds between O2G and water hydrogen atoms are somehow repelled by the strong positively charged Mg^{2+}, and the distance of the peak distribution is farther than the one of O3G, which is free from Mg^{2+} coordination. The second and third water shells are more clearly shown in the distribution function of O2G than of O3G. This can be the effect of coordination of Mg^{2+} to surrounding water molecules to arrange them more structurally. The distribution function of atom O2B, which is also coordinated by Mg^{2+}, is very similar to that of O2G, and all other oxygen atoms of the triphosphate follow the characteristics of O3G, except that oxygen atoms in α- and β-phosphates have lower peaks due to the less accessible area for water molecules. The most dramatic peak for strongly charged Mg^{2+} indicates even more water molecules can be coordinated simultaneously. A zero density region for Mg^{2+} around 3 Å clearly shows that the first water shell is very tightly bound, thus excluding second shell neighbors from invading the first shell.

Different threshold distances were applied for different atoms of Mg·ATP to count the average number of hydrogen bonds or salt bridges coordinated by each atom of the molecule. We used the typical hydrogen bond lengths available in the literature (for example, see Stryer 1995) plus 0.1 Å as the thresholds to determine how many water molecules are hydrogen bonded. From the observation of the distribution function shown in Fig. 4 we used a threshold of 2.2 Å for Mg^{2+}. Table 1 shows the thresholds and numbers of coordinated water molecules of atoms able to form hydrogen bonds (or salt bridges for Mg^{2+}) averaged over a 2-ns trajectory. The data in this table show that most of the hydrogen bonds are in the triphosphate, especially the γ-phosphate.

When Mg·ATP enters the binding site, many hydrogen bonds originally formed with water molecules switch to protein residues. Many crystal structures have demonstrated that the protein residues which bind to the triphosphate are highly conserved indicating that these residues play a key role in recognizing the corresponding hydrogen binding sites of Mg·ATP. The phosphates form hydrogen bonds with originally distant catalytic residues to "pull" them together, and all these hydrogen bonds collectively drive the power stroke of the enzyme.

Table 1 Average number of water molecules coordinated by the atoms of Mg·ATP and the corresponding threshold distances to decide the coordination

Group	Adenine						Ribosome					
Atom	N1	N3	N6	H61	H62	N7	O2'	H2'	O3'	H3T	O4'	O5'
Threshold (Å)	2.98	2.98	3.14	2.14	2.14	2.98	2.7	1.74	2.7	1.74	2.7	2.7
#No. of H_2O	0.54	0.49	1.40	0.39	0.41	0.76	0.63	0.30	0.81	0.25	0.22	0.21
Group		α-Phosphate			β-Phosphate			γ-Phosphate				
Atom		O1A	O2A	O3A	O1B	O2B	O3B	O1G	O2G	O3G	MG	
Threshold (Å)		2.7	2.7	2.7	2.7	2.7	2.7	2.7	2.7	2.7	2.2	
#No. of H_2O		2.25	2.40	0.30	2.30	2.13	0.22	2.75	2.56	2.98	3.87	

The γ-phosphate is especially important for the function of the enzyme. According to our estimate, this phosphate has the ability to form about eight hydrogen bonds, and yet after hydrolysis the negatively charged Pi and the negatively charged ADP repel each other. The repulsion separates the cleaved Pi and ADP, both of which remain temporarily bound to different parts of the protein. As shown in Appendix F, Mg·ADP is even harder to deform than Mg·ATP. The shortening of the molecule due to the absence of the γ-phosphate and the change in the elastic properties contribute to the different mechanical roles in the binding site between Mg·ATP and Mg·ADP. Thus, the γ-phosphate plays a central role in elastically deforming distant residues during binding, and then relieving the stress through hydrolysis.

Acknowledgements JCL was supported by NSF Grant DMS-9972826; DC was supported by NSF Grant CHE-0078458; SS and GO was supported by NIH Grant GM59875–02. Computational resources were provided by an equipment grant from DOE Office of Basic Energy Sciences #DE-FG03–87ER13793. The authors thank Albert Mildvan, Todd J. Minehardt, Hongyun Wang, Aaron Dinner, Oleg Igoshin, and Iris Antes for valuable discussions during the course of this work.

Appendix A: atom numbers

The atom numbers used in this report are shown in Fig. 5.

Appendix B: methods

Simulations of Mg·ATP in water were carried out using the molecular dynamics program CHARMM (Brooks et al. 1983; MacKerell et al. 1998). We performed two different sets of simulations, one using the original partial charge distributions provided in CHARMM (Pavelites et al. 1997), and the other using the partial charge distributions derived by Minehardt (Minehardt et al. 2002). Both simulations used the same Mg^{2+} parameters from CHARMM version 27. The simulations were carried out in a cube 31.1 Å on a side, containing 1,000 TIP3P water molecules. Periodic boundary conditions were imposed using Ewald sums (Billing et al. 1996; Frenkel et al. 2002). Atom O5' (as shown in Fig. 5) was harmonically constrained and the size of the water box was chosen so that the ATP molecule is free to rotate without contacting the boundary of the box. The number of water molecules was such that the bulk density of water is 1 g cm^{-3}. Using a shifted potential and the SHAKE algorithm (Ryckaert et al. 1977), the long-range non-bonded interactions were limited to 13 Å. The Verlet leapfrog algorithm was used for numerical calculations using a time step of 1 fs (Hockney et al. 1988). The system was first minimized by the adopted basis Newton–Raphson method for 100 steps (Brooks et al. 1983). After the energy minimization, the system was heated from 0 K to 300 K over the course of 15 ps, and then equilibrated at 300 K for 30 ps. Simulation runs of 1 ns or more were then carried out after equilibration.

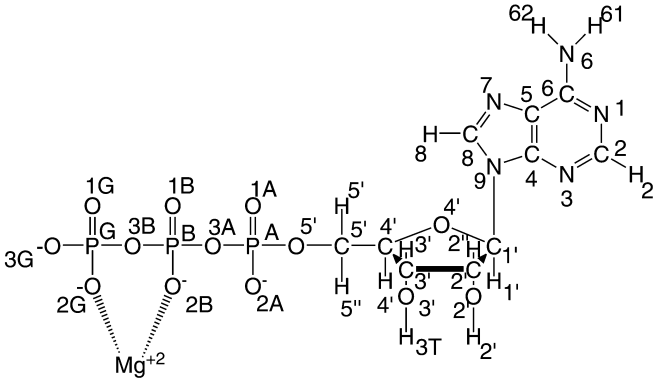

Fig. 5 The chemical structure of Mg·ATP. Atom numbers are the same as in CHARMM

To obtain free energy functions, umbrella sampling was employed and the overall free energy function was obtained by combining statistics from different regions (Ferrenberg et al. 1989). The θ–Φ plane was partitioned into 21 regions to apply the umbrella sampling method with different potentials. The quadratic potential function

$$E = \frac{1}{2}\left[k_\theta(\theta-\theta_0)^2 + k_\phi\left(\phi-\phi_0^2\right)\right]$$

was used to fit the potentials. The centers (θ_0, Φ_0) of the potential functions in these 21 regions are listed in Table 2.

The potential coefficients $k_\theta = 6$ kcal mol^{-1}, $k_\Phi = 6$ kcal mol^{-1} were used for the first two rows of potentials. For the last row, Φ is close to $\pi/2$, where the circumferential angle θ is not defined, so we added a steep exponential function to avoid sampling too close to $\Phi = \pi/2$. The potential functions for umbrella sampling of the bottom row were

$$E = \frac{1}{2}\left[k_\theta(\theta-\theta_0)^2 + k_\phi\left(\phi-\phi_0^2\right)\right] + e^{-\alpha(\phi-\phi_0)}$$

where $\alpha = 8$ kcal mol^{-1} was chosen to bias the potential. Stronger potentials of $k_\theta = 16$ kcal mol^{-1} and $k_\Phi = 10$ kcal mol^{-1} were also applied to enhance the avoidance of divergent sampling at $\Phi = \pi/2$. In the Φ direction

Table 2

(θ, Φ) (rad)						
(−2.69, 0.17)	(−1.8, 0.17)	(−0.89, 0.17)	(0, 0.17)	(0.89, 0.17)	(1.8, 0.17)	(2.69, 0.17)
(−2.69, −0.52)	(−1.8, −0.52)	(−0.89, −0.52)	(0, −0.52)	(0.89, −0.52)	(1.8, −0.52)	(2.69, −0.52)
(−2.69, −1.22)	(−1.8, −1.22)	(−0.89, −1.22)	(0, −1.22)	(0.89, −1.22)	(1.8, −1.22)	(2.69, −1.22)

Φ_0 was set as −1.4 rad so that the effective minimum after adding the exponential term was at $\Phi_0 = -1.22$, as proposed in the table. The procedure of the umbrella sampling simulation, including the algorithm, periodic boundary conditions with Ewald sums, minimization, and the equilibration process, is the same as described for standard MD simulations. The simulation runs of 1 ns were carried out for each sampling region.

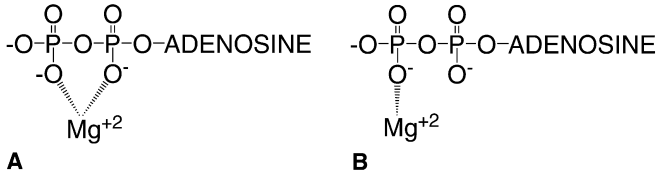

Fig. 6A, B Coordinations of Mg^{2+}. **A** ADP: in simulation, experimental results, and some crystal structures. **B** ADP: in several crystal structures

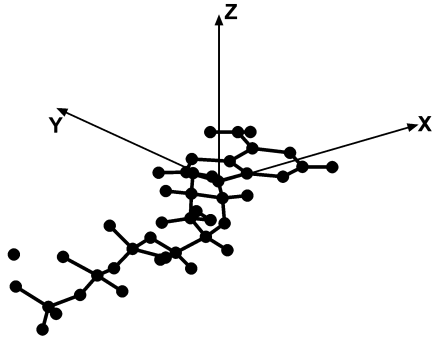

Fig. 7 Stick representation showing the coordinate system used to interpret our simulations

Appendix C: coordination of the Mg^{2+} for ADP

We carried out simulations of Mg·ADP in water, using the Minehardt parameter set. The results show that Mg^{2+} always coordinates one oxygen atom from the β-phosphate, one oxygen atom from the α-phosphate, and four water molecules (Fig. 6A). This coordination agrees with the experimental results of Mg·ADP in water (Bridger et al. 1983). That is, in order to hydrolyze Mg·ATP, the original coordination to the γ-phosphate must be removed. The crystal structures of Mg·ADP bound enzymes demonstrate that, in many cases, Mg^{2+} only coordinates one oxygen atom from β-phosphate (Fig. 6B), although in some cases it also coordinates with oxygen atoms of α and β-phosphates (Fig. 6A).

Appendix D: bowl shape trajectory of the γ-phosphorus

In order to describe the various conformations of the Mg·ATP molecule, a body-fixed coordinate system was used. MD trajectories show that the major conformational changes of the molecule involve rotations about the phosphoanhydride bonds that form the long axis of the molecule. The adenine ring does not experience significant distortions. Therefore, we place our reference frame on the adenine ring, with the origin located at nitrogen atom N9 in the adenine linking the carbon

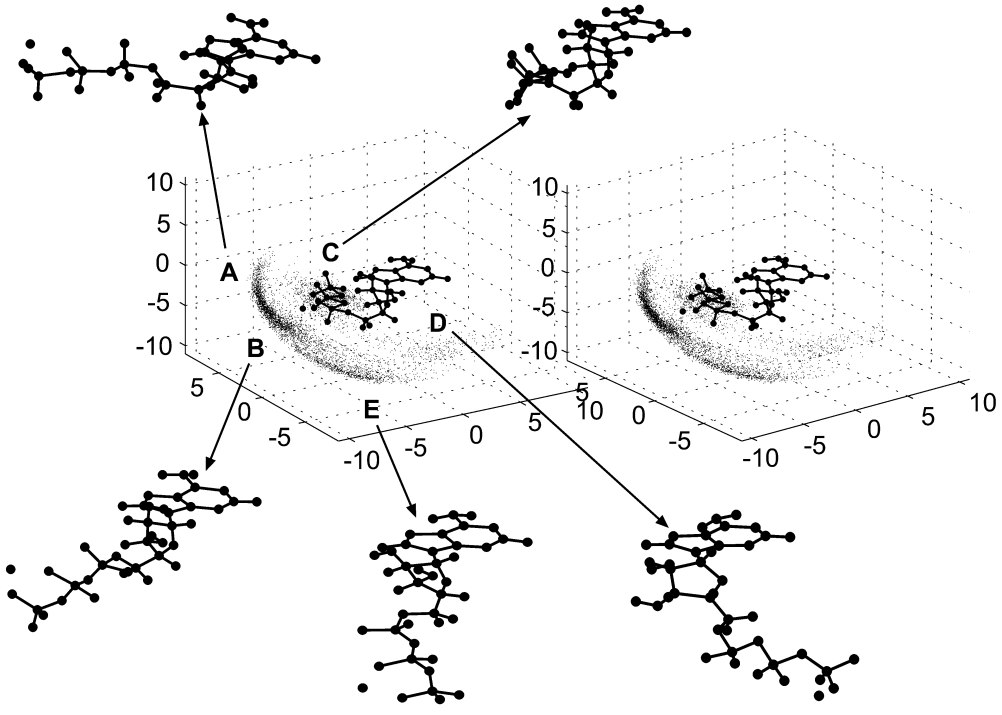

Fig. 8 A stereo view of points visited during a 1 ns trajectory shown in the Cartesian coordinate system adapted to the nucleotide. Using the adenine ring as a reference frame, each dot represents the location of the γ-phosphorus of Mg·ATP at 0.1-ps intervals. Five different configurations of Mg·ATP corresponding to the higher populations of atomic configurations labeled ABCDE are also shown. The orientation is transformed so that the adenine ring is nearly horizontal for all the configurations

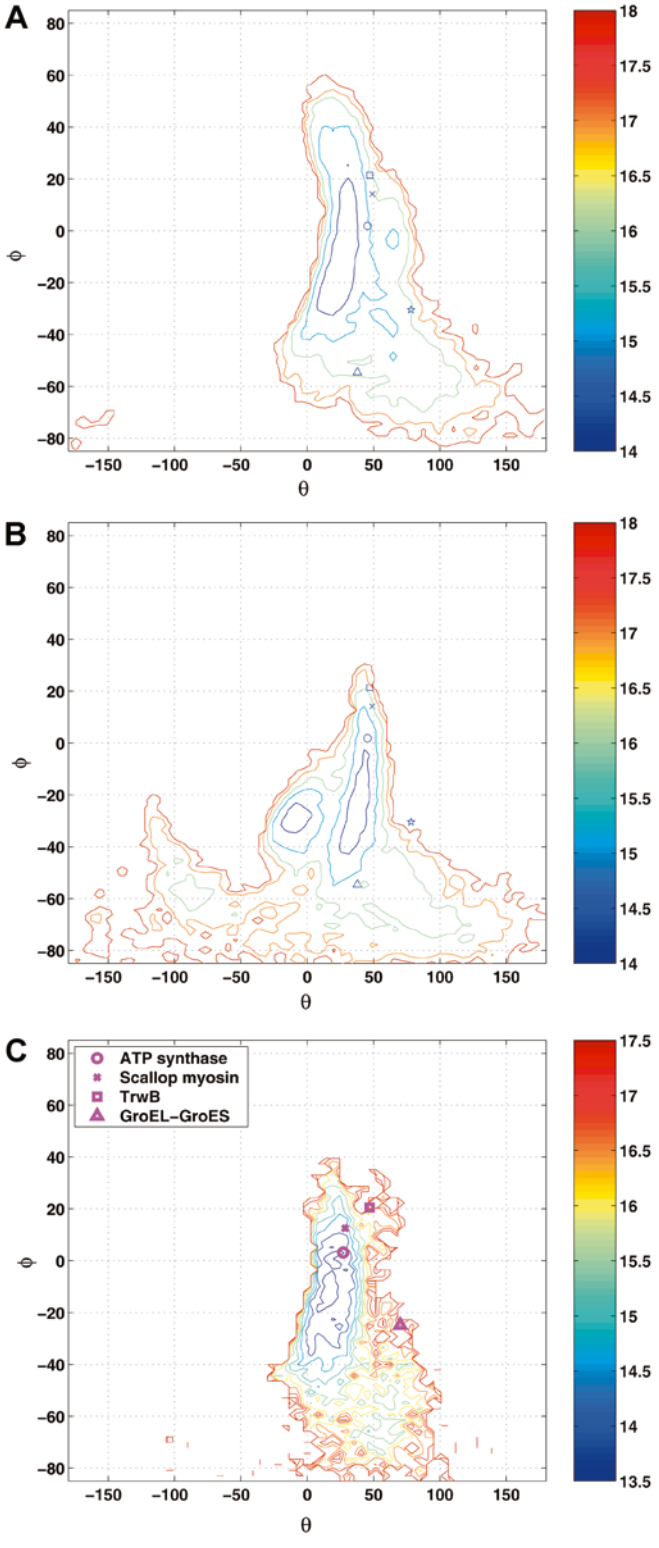

Fig. 9A–C The free energy (in units of k_BT) contours over the θ–Φ plane. **A** The free energy contour for Mg·ATP in water using CHARMM parameters. B The free energy contour for Mg·ATP in water using Minehardt parameters. **C** The free energy contour for Mg·ADP in water using Minehardt parameters. Locations of the β-phosphorus for several ADP molecules in different crystal structures are marked

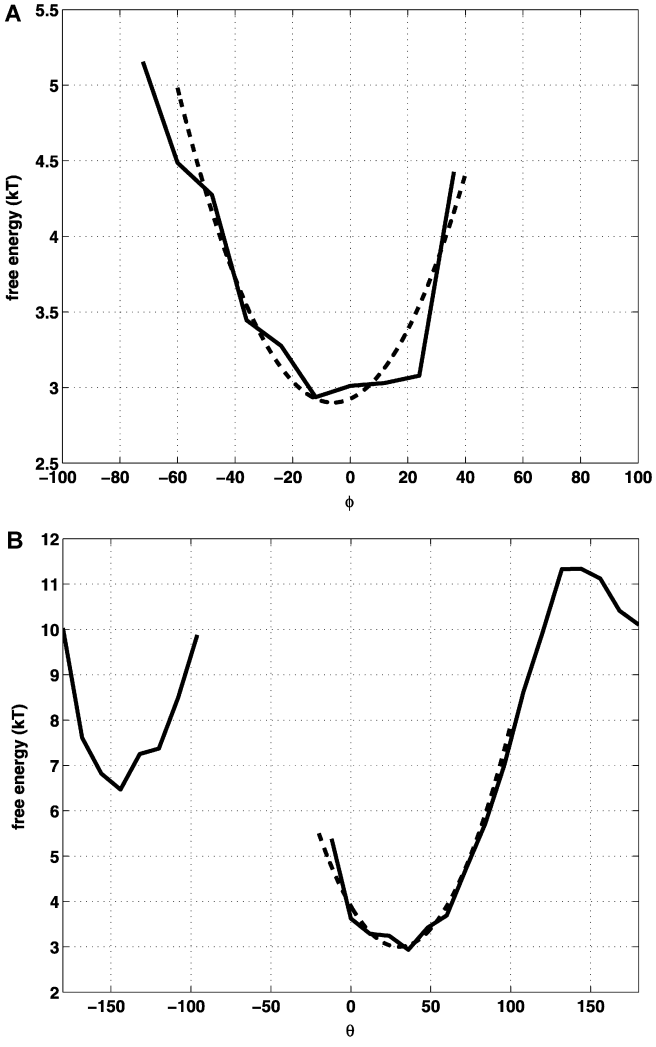

Fig. 10A, B Cross-sections of the free energy surface for Mg·ATP and the fitted parabolic curves used to determine the effective elastic constants. **A** The cross-section of the free energy at constant θ for Mg·ATP. **B** The cross-section of free energy at a constant Φ

atom in the ribose, as shown in Fig. 7. The x-axis lies along the direction from atom N9 to atom C4, with the adenine ring lying in the x–y plane, and the z-axis perpendicular to it.

Figure 8 shows a stereo view of points visited during a 1-ns trajectory within the body-fixed coordinate frame using the Minehardt parameter set. Each dot represents the location of the γ-phosphorus in a Cartesian coordinate system with the origin at the center of the adenine, and x–y plane parallel to that of the adenine ring. Configurations shown are sampled every 0.1 ps. Five regions (labeled ABCDE) are assigned in the figure with higher populations of atomic configurations. The configurations of the ATP molecule in these five regions are also shown. Figure 8 also shows that the trajectory points form a "bowl" shape, suggesting that the motion can be described by a simple spherical coordinate system.

Appendix E: free energy contours from molecular dynamics

The free energy contours for Mg·ATP and Mg·ADP obtained from straightforward 1-ns MD simulations in the θ–Φ plane are shown in Fig. 9. For Mg·ADP, the trajectory of the β-phosphorus, instead of the γ-phosphorus for Mg·ATP, is used to define the two collective coordinates. The overall free energy surfaces of Mg·ATP in water using different sets of parameters are different, while the regions of the minimum free energy and the pattern around the free energy wells of both cases are similar. The free energy surfaces of Mg·ADP in water and Mg·ATP in water are very similar, indicating that, in terms of the θ–Φ coordinates, the properties of the molecules are close to each other. Because the results were obtained by direct MD simulations, the sampling may be stuck at a certain region, and thus umbrella sampling reflects better statistics. For the simulation of Mg·ADP, the locations of crystal structures mapped to θ–Φ plane are also shown in Fig. 9.

Appendix F: estimation of elastic properties

We locate the minimum free energy in Fig. 3, and estimate the surface shape around the minimum by cutting cross-sections of constant θ and Φ. Figure 10A shows the cross-section of the free energy surface at $\theta = 36°$, and Fig. 10B shows the cross-section of the free energy surface at $\Phi = -12°$, for Mg·ATP with CHARMM parameters. Although the curves are rough and slightly asymmetric, they can be approximated by a parabola up to 1.5–2 k_BT above the free energy minimum, as shown in the figure. From this we obtain that the effective elastic constant in the Φ direction (keeping θ constant) is about 4.69 k_BT rad^{-2}. That is, with the radius of motion of about 8.8 Å for Mg·ATP, the elastic constant k_Φ for Mg·ATP in solution around the minimum free energy regions are about 25 pN nm^{-1}. Similarly, we fit a parabolic curve to estimate the effective elastic constant k_θ in the θ direction as 35 pN nm^{-1} for Mg·ATP, showing that the molecule is stiffer in the θ direction than in the Φ direction. The same procedure can be used to estimate the elastic properties of Mg·ADP. From Fig. 9C, we obtain that k_Φ of Mg·ADP is 7.6 k_BT rad^{-2}, or 74 pN nm^{-1}, and k_θ of Mg·ADP is 24.6 k_BT rad^{-2}, or 239 pN nm^{-1}.

References

Billing G et al (1996) Introduction to molecular dynamics and chemical kinetics. Wiley, New York, xii, 183 pp

Bridger W et al (1983) Cell ATP. Wiley, New York, x, 170 pp

Brooks BR et al (1983) Charmm—a program for macromolecular energy, minimization, and dynamics calculations. J Comput Chem 4(2):187–217

Chandler D (1987) Introduction to modern statistical mechanics. Oxford University Press, New York, xiii, 274 pp

Cohn M et al (1962) Nuclear magnetic resonance spectra of adenosine di- and triphosphate. 2. Effect of complexing with divalent metal ions. J Biol Chem 237(1):176–181

Ferrenberg A et al (1989) Optimized Monte-Carlo data analysis. Phys Rev Lett 63(12):1195–1198

Frenkel D et al (2002) Understanding molecular simulation: from algorithms to applications. Academic, San Diego, Calif., xxii, 638 pp

Hockney RW et al (1988) Computer simulation using particles. Adam Hilger, Bristol, UK, xxi, 540 pp

Kuntz G et al (1973) Contrasting structures of magnesium and calcium adenosine-triphosphate complexes as studied by nuclear relaxation. Fed Proc 32(3):546–552

MacKerell AD Jr et al (1998) CHARMM: the energy function and its parameterization with an overview of the program. In: Schleyer PvR (ed) Encyclopedia of computational chemistry. Wiley, New York, pp 271–277

Mildvan A (1987) Role of magnesium and other divalent cations in ATP-utilizing enzymes. Magnesium 6:28–33

Minehardt TJ et al (2002) A classical and ab initio study of the interaction of the myosin triphosphate binding domain with ATP. Biophys J 82(2):660–675

Pavelites JJ et al (1997) A molecular mechanics force field for NAD^+, NADH, and the pyrophosphate groups of nucleotides. J Comput Chem 18(2):221–239

Ryckaert JP et al (1977) Numerical-integration of cartesian equations of motion of a system with constraints—molecular-dynamics of N-alkanes. J Comput Phys 23(3):327–341

Stryer L (1995) Biochemistry. WH Freeman, New York, xxxiv, 1064 pp

Sun S et al (2003) Elastic energy storage in ß-sheets with application to F1-ATPase. Eur J Biophys (in press)

Wang H et al (1998) Energy transduction in the F1 motor of ATP synthase. Nature (London) 396(6708):279–282